A central role for DOCK2 during interstitial lymphocyte motility and sphingosine-1-phosphate–mediated egress

César Nombela-Arrieta,[1] Thorsten R. Mempel,[2] Silvia F. Soriano,[1] Irina Mazo,[2] Matthias P. Wymann,[3] Emilio Hirsch,[4] Carlos Martínez-A.,[5] Yoshinori Fukui,[6] Ulrich H. von Andrian,[2] and Jens V. Stein[1]

[1]Theodor Kocher Institute, University of Bern, CH-3012 Bern, Switzerland
[2]The Center for Blood Research and Department of Pathology, Harvard Medical School, Boston, MA 02115
[3]Department of Clinical Biological Sciences, Institute of Biochemistry and Genetics, University of Basel, CH-4003 Basel, Switzerland
[4]Department of Genetics, Biology and Biochemistry, University of Turin, 10060 Turin, Italy
[5]Department of Immunology and Oncology, National Center for Biotechnology-CSIC, 28049 Madrid, Spain
[6]PRESTO, Japan Science and Technology Agency, and Division of Immunogenetics, Department of Immunobiology and Neuroscience, Medical Institute of Bioregulation, Kyushu University, Fukuoka, 812-8582, Japan

Recent observations using multiphoton intravital microscopy (MP-IVM) have uncovered an unexpectedly high lymphocyte motility within peripheral lymph nodes (PLNs). Lymphocyte-expressed intracellular signaling molecules governing interstitial movement remain largely unknown. Here, we used MP-IVM of murine PLNs to examine interstitial motility of lymphocytes lacking the Rac guanine exchange factor DOCK2 and phosphoinositide-3-kinase (PI3K)γ, signaling molecules that act downstream of G protein–coupled receptors, including chemokine receptors (CKRs). T and B cells lacking DOCK2 alone or DOCK2 and PI3Kγ displayed markedly reduced motility inside T cell area and B cell follicle, respectively. Lack of PI3Kγ alone had no effect on migration velocity but resulted in increased turning angles of T cells. As lymphocyte egress from PLNs requires the sphingosine-1-phosphate (S1P) receptor 1, a $G_{\alpha i}$ protein–coupled receptor similar to CKR, we further analyzed whether DOCK2 and PI3Kγ contributed to S1P-triggered signaling events. S1P-induced cell migration was significantly reduced in T and B cells lacking DOCK2, whereas T cell–expressed PI3Kγ contributed to F-actin polymerization and protein kinase B phosphorylation but not migration. These findings correlated with delayed lymphocyte egress from PLNs in the absence of DOCK2 but not PI3Kγ, and a markedly reduced cell motility of DOCK2-deficient T cells in close proximity to efferent lymphatic vessels. In summary, our data support a central role for DOCK2, and to a lesser extent T cell–expressed PI3Kγ, for signal transduction during interstitial lymphocyte migration and S1P-mediated egress.

CORRESPONDENCE
Jens V. Stein:
jstein@tki.unibe.ch

Abbreviations used: ANOVA, analysis of variance; CKR, chemokine receptor; GPCR, G protein–coupled receptor; HEV, high endothelial venule; MP-IVM, multiphoton intravital microscopy; o.n., overnight; PI3K, phosphoinositide-3-kinase; PKB, protein kinase B; PLN, peripheral lymph node; RGS, regulator of G protein signaling; S1P, sphingosine-1-phosphate; SLO, secondary lymphoid organ; WGA, wheat germ agglutinin.

Blood-borne naive lymphocytes continuously enter secondary lymphoid organs (SLOs), such as peripheral lymph nodes (PLNs) and spleen, where they screen APCs in search of their cognate antigen. In absence of inflammation, lymphocytes leave PLNs after an average dwell time of 12–24 h to enter lymphatic vessels located in the lymph node medulla (1, 2). Efferent lymph vessels carry lymphocytes back into the blood circulation from where they reinitiate their recirculation pathway. Their long life span and constant migration through SLOs make lymphocytes one of the most motile mammalian cell types (1, 2). Together with adhesion receptor molecules, two subfamilies of lymphocyte-expressed G protein–coupled receptors (GPCRs) are known to guide lymphocyte trafficking: chemokine receptors (CKR), including CCR7, CXCR4, and CXCR5, and the sphingosine-1-phosphate (S1P) receptor 1, $S1P_1$ (1, 2).

SLO-expressed homeostatic chemokines, such as the CCR7 ligands CCL19 and CCL21, the CXCR5 ligand CXCL13, and the CXCR4

C. Nombela-Arrieta and T.R. Mempel contributed equally to this work.

The online version of this article contains supplemental material.

ligand CXCL12, fulfill two functions during lymphocyte trafficking. First, they are presented on high endothelial venules (HEVs) where they promote firm arrest of blood-borne lymphocytes (1–5). Second, chemokines organize lymphoid tissue by creating specific microenvironments. Transmigrated CCR7^{high} T cells move to the PLN paracortex correlating with CCL21 and CCL19 expressed at high concentrations in this area, whereas CXCR5-expressing B cells accumulate in follicles where high levels of CXCL13 are present (1–3). Accordingly, mice lacking homeostatic chemokines or their receptors show disturbed SLO architecture, with poorly developed T and B cell areas (6–9).

The recent establishment of multiphoton intravital microscopy (MP-IVM) has allowed investigators to directly visualize the dynamics of lymphocyte motility within their microenvironments of primary and secondary lymphoid tissues (10–15). Somewhat unexpectedly, most nonactivated naive lymphocytes display a highly motile behavior that has been described as random walk (11–15). In fact, lymphocytes appear to use stromal cell networks as guidance cues for their migration paths (16). Continuous lymphocyte motility may have evolved to increase "antigen scanning efficiency" and, as a consequence, the likelihood of productive APC–lymphocyte encounters. It is currently unclear whether chemokines or additional tissue-derived factors are responsible for lymphocyte motility observed in lymphoid tissue. Interestingly, in two-dimensional in vitro assay systems, chemokines can increase random motility in apparent absence of gradients (17, 18), and studies in B cells lacking the $G_{\alpha i2}$ subunit and regulator of G protein signaling (RGS)1 have uncovered a central role for GPCR signaling during interstitial migration (19).

In the absence of inflammation, lymphocytes exit PLNs through lymphatic sinuses located in the medulla of PLNs (1, 2). S1P receptor 1 ($S1P_1$) is a $G_{\alpha i}$-coupled receptor, which, together with its ligand, has been implicated in the regulation of lymphocyte egress (1, 20). First evidence for a role of S1P came from pharmacological studies using an S1P analogue, FTY720, which in its phosphorylated form (FTY720-P) acts as a strong agonist on four out of five known S1P receptors, including $S1P_1$ (20, 21). FTY720 administration leads to a severe block of lymphocyte egress from PLNs, with concomitant blood lymphopenia (21, 22). In lymphocytes, FTY720 induces $S1P_1$ internalization and a long-lasting state of nonresponsiveness to S1P (23, 24). Likewise, $S1P_1$-deficient thymocytes are unable to egress from the thymus, and when adoptively transferred into recipient mice, mature $S1P_1$-deficient thymocytes accumulate in PLNs but are unable to exit these or any other SLO (24, 25). Despite its importance, very little is known about S1P-induced intracellular signaling pathways in lymphocytes.

DOCK2 is a hematopoietic cell–specific member of the CDM (CED-5 in *Caenorhabditis elegans*, DOCK180 in man, and myoblast city in *Drosophila melanogaster*) family of proteins, which functions as a guanine exchange factor for the small GTPase Rac (26–28). Rac is a key regulator of cell motility by controlling F-actin polymerization and lamellipodia formation (29). In the absence of DOCK2, chemokine-induced F-actin polymerization, directed in vitro migration to chemokine gradients, and short-term homing are strongly impaired in T and B cells, despite similar CKR surface expression levels (30, 31). A DOCK2-independent, phosphoinositide-3-kinase (PI3K)-dependent residual chemotactic response nonetheless exists in lymphocytes, which during in vitro migration requires PI3Kγ in T cells, whereas the PI3Kδ isoform appears to be predominant in B cells (31, 32). Accordingly, PI3Kγ-deficient T but not B cells show a mild reduction in their homing efficiency to SLOs. T cells lacking both DOCK2 and PI3Kγ show a virtually abolished migration to chemokines in vitro and have a further reduced homing capacity toward SLOs (31).

Although the roles of DOCK2 and PI3Kγ during chemokine-mediated lymphocyte migration in vitro and lymphocyte homing from blood to SLOs in vivo are well described, it was unclear whether and how these molecules would affect velocity and directionality of interstitially migrating lymphocytes. We have therefore investigated the role of both molecules by directly comparing the migratory behavior of adoptively transferred control, DOCK2$^{-/-}$, PI3Kγ$^{-/-}$, or DOCK2$^{-/-}$ × PI3Kγ$^{-/-}$ T and B cells inside the PLNs of anesthetized mice using MP-IVM, as described previously (33). Our findings show that cells lacking DOCK2 display a strongly reduced interstitial motility with decreased translocation speed and increased turning angles, resulting in a low motility coefficient. In contrast, T cell directionality was only mildly affected in the absence of PI3Kγ. Finally, we also address the function of DOCK2 and PI3Kγ in S1P-stimulated T and B cells in vitro and during lymph node egress in vivo, using egress assays and MP-IVM of PLN medulla.

RESULTS

Intranodal motility of T cells in the absence of DOCK2 and PI3Kγ

T cell migration along chemokine gradients in vitro, as well as homing to SLOs in vivo, requires DOCK2-induced Rac activation (30), with a residual PI3Kγ-dependent contribution (31, 32). To investigate how the lack of DOCK2 and/or PI3Kγ influenced interstitial motility of lymphocytes that had successfully entered lymphoid tissue, we adoptively transferred purified control T cells together with DOCK2$^{-/-}$, PI3Kγ$^{-/-}$, or DOCK2$^{-/-}$ × PI3Kγ$^{-/-}$ T cells differentially labeled with CFSE or CMTMR. To compensate for the reduced accumulation of DOCK2-deficient T cells in PLNs (30, 31), two to four times more of these cells were injected compared with control cells. After 15–22 h, direct imaging of the T cell area of popliteal lymph nodes was performed using MP-IVM (33), and the in situ interstitial migratory behavior of transferred control and gene-deficient lymphocytes was compared during 30-min periods within the same field of view. Flow cytometry analysis of transferred control and DOCK2-deficient lymphocytes recovered from PLNs revealed that both populations consisted of 70–90% L-selectin^{high} CD44^{low} LFA-1^{intermediate} CD45RB^{high} cells,

indicative of bona fide naive lymphocytes. The remaining cells were L-selectin^{high} CD44^{high} LFA-1^{intermediate} CD45RB^{high} central memory–like T cells, which were more frequent in the absence of DOCK2 (12 ± 4% vs. 29 ± 2% control and DOCK2$^{-/-}$ T cells, respectively; Fig. S1, available at http://www.jem.org/cgi/content/full/jem.20061780/DC1). We did not observe a bimodal migratory behavior within control or DOCK2-deficient lymphocyte populations in our experiments (see below), suggesting that naive and central memory–like populations have comparable motility.

As reported (11, 33), control T cells vigorously migrated in what appeared a random walk pattern, frequently entering and leaving the field of view during the observation period. In contrast, most DOCK2$^{-/-}$ T cells oscillated around the initial tracking spot, unable to initiate steady movement in any direction (Fig. 1 A). Of note, most DOCK2$^{-/-}$ T cells still underwent continuous shape changes and emitted cell projections that appeared to correspond to the formation of a transient leading edge (Videos S1 and S2, available at http://www.jem.org/cgi/content/full/jem.20061780/DC1). Alternatively, the apparent residual shape changes of DOCK2-deficient cells could have resulted, at least in part, from collisions with highly motile endogenous cells. Although control T cells traveled with a median instantaneous three-dimensional velocity of 12.6 ± 0.7 μm/min (mean ± SD), DOCK2$^{-/-}$ T cells moved with 7.0 ± 0.1 μm/min (Fig. 1 B). As the instantaneous three-dimensional velocity is calculated on the basis of the frame to frame changes of single cell centroid positions, small displacements or shape changes are also included. This could account for the fact that DOCK2 deficiency induced a less remarkable reduction in the mean instantaneous three-dimensional velocity than predicted from the three-dimensional trajectories of DOCK2$^{-/-}$ T cells (Fig. 1 A). We occasionally observed DOCK2$^{-/-}$ T cells migrating comparably to control T cells in terms of displacement and speed (Videos S1 and S2), indicating that DOCK2-independent pathways controlling cell migration are present in rare T cells.

The erratic oscillations of DOCK2$^{-/-}$ T cells around the initial tracking spot are reflected by the turning angle frequency distribution, indicating decreased directionality (Fig. 1 C). To account for both instantaneous three-dimensional

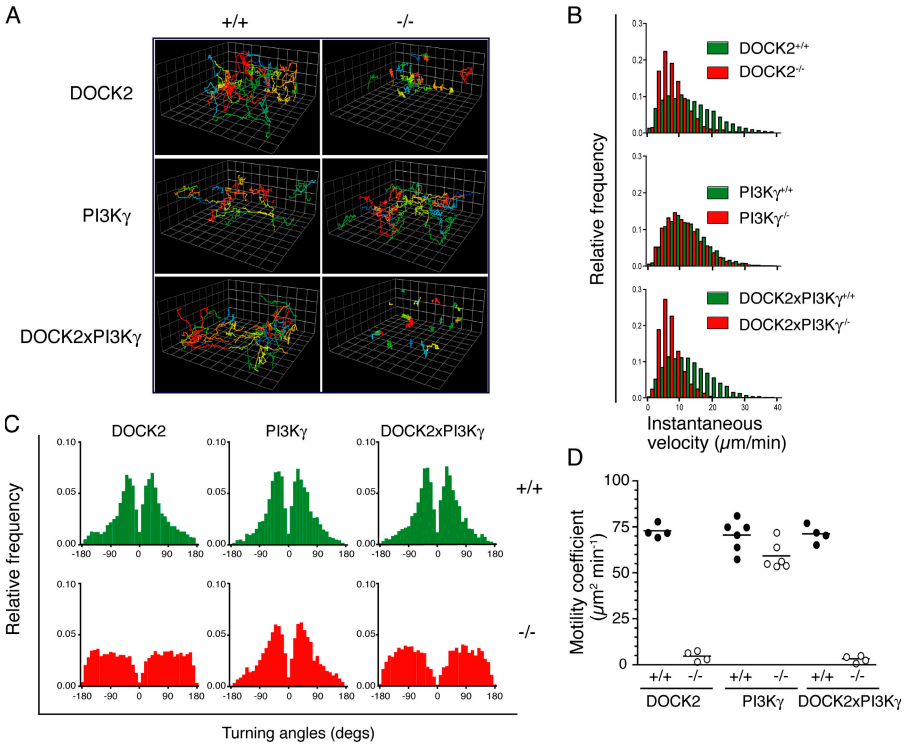

Figure 1. Paracortical T cell migration in the absence of DOCK2 and PI3Kγ. Fluorescently labeled control T cells and DOCK2$^{-/-}$, PI3Kγ$^{-/-}$, or DOCK2$^{-/-}$ × PI3Kγ$^{-/-}$ T cells were adoptively transferred into wild-type recipients, and their migratory behavior inside popliteal lymph nodes was analyzed using MP-IVM. The grid length of each square corresponds to 20.8 μm. (A) Representative three-dimensional tracks of control T cells (+/+; left column) and DOCK2$^{-/-}$, PI3Kγ$^{-/-}$, or DOCK2$^{-/-}$ × PI3Kγ$^{-/-}$ T cells (−/−; right column) over 30-min periods. Each colored line represents a single T cell track. (B) Velocity profiles of control T cells (green bars) and DOCK2$^{-/-}$, PI3Kγ$^{-/-}$, or DOCK2$^{-/-}$ × PI3Kγ$^{-/-}$ T cells (red bars). Histograms show the relative frequency distribution of different populations compared with control T cells. (C) Turning angles of control T cells (+/+; top green panel) and DOCK2$^{-/-}$, PI3Kγ$^{-/-}$, or DOCK2$^{-/-}$ × PI3Kγ$^{-/-}$ T cells (−/−; bottom red panel). The wider angle distribution of DOCK2-deficient T cells is indicative of less directed cell movement. (D) Motility coefficients of T cells in the presence or absence of DOCK2 and/or PI3Kγ. Each dot represents the combined motility coefficient of one experiment. Filled dots, control T cells; empty dots, genetically deficient T cells. The bars indicate mean values. The statistical analysis is summarized in Table I.

velocity and turning angle distribution, we determined the motility coefficient for control and DOCK2$^{-/-}$ T cells as a measure of area scanning efficiency per time unit (Fig. 1 D) (12). In the absence of DOCK2, the motility coefficient decreased to 4.8 ± 2.8 μm^2/min, reflecting the scarce displacements of DOCK2$^{-/-}$ T cells. Control T cells, on the other hand, had an ∼15-fold higher motility coefficient of 72.9 ± 3.7 μm^2/min, in line with previous reports (13, 33). All MP-IVM motility parameters are summarized in Table I.

To analyze the role of PI3Kγ during lymphocyte intranodal motility, we performed MP-IVM experiments comparing purified control and PI3Kγ$^{-/-}$ T cells. In six 30-min videos analyzed, PI3Kγ$^{-/-}$ T cells showed no significant reduction of the median instantaneous three-dimensional velocity (PI3Kγ$^{+/+}$ T cells, 11.5 ± 0.8 μm/min; PI3Kγ$^{-/-}$ T cells, 11.0 ± 1.3 μm/min; Fig. 1 B and Video S3, which is available at http://www.jem.org/cgi/content/full/jem.20061780/DC1). However, a more thorough comparison of turning angles uncovered a slight shift toward wider turning angles in the absence of PI3Kγ. This observation indicates that PI3Kγ$^{-/-}$ T cells undergo more abrupt directional changes during interstitial migration compared with control cells (Fig. 1 C), which is reflected in the minor but significant reduction of the PI3Kγ$^{-/-}$ T cell motility coefficient (59.2 ± 7.3 compared with 70.6 ± 8.5 μm^2/min of control cells; Fig. 1 D and Table I).

In homing experiments, both DOCK2 and, to a minor extent, PI3Kγ contribute to efficient T cell accumulation in PLNs (31). We set out to analyze the combined effect of these signaling molecules on lymphocyte motility inside PLNs. Adoptively transferred DOCK2$^{-/-}$ × PI3Kγ$^{-/-}$ T cells behaved comparably to T cells lacking only DOCK2, remaining essentially stationary during the observation period (Table I and Videos S4 and S5, which are available at http://www.jem.org/cgi/content/full/jem.20061780/DC1). Collectively, these observations reveal a central role for DOCK2, and to a lesser extent PI3Kγ, during signal transduction of tissue-derived promigratory signals causing efficient interstitial T cell motility.

DOCK2 but not PI3Kγ controls B cell motility inside the follicles

B cell migration to chemokines in vitro requires DOCK2 and a PI3K isoform different from PI3Kγ (31, 32). We therefore investigated the influence of DOCK2 on B cell random motility using MP-IVM. In the absence of DOCK2, B cell homing to PLNs is further diminished compared with DOCK2$^{-/-}$ T cells due to the B cell–specific requirement for DOCK2 during efficient integrin activation (31). However, when transferring three to five times more purified DOCK2$^{-/-}$ B cells compared with control B cells, we were able to observe a sufficient number of gene-deficient cells for a meaningful analysis of their migratory behavior (Table I). As for T cells, transferred control and DOCK2-deficient B cells were >90% L-selectin^{high} (not depicted).

15–22 h after transfer, most transferred B cells, regardless of DOCK2 expression, were detected in external areas of the lymph nodes in close proximity to the subcapsular sinus, where B cell follicles are located. Compared with T cells, control B cells displayed a lower median instantaneous three-dimensional velocity (7.9 ± 0.8 μm/min). An examination of frequency histograms of three-dimensional velocities revealed a reduction in DOCK2$^{-/-}$ B cell translocation speed to a mean velocity of 5.2 ± 0.9 μm/min (Fig. 2 B and Table I). Importantly, individual three-dimensional cell tracks reflect the severely compromised displacement of DOCK2$^{-/-}$ B cells during the observation period, although some cells were observed emitting cell membrane projections, similar to DOCK2$^{-/-}$ T cells (Fig. 2 A). The continuous changes in direction and oscillations around the initial tracking spot resulted in increased turning angles and a strongly reduced motility coefficient (1.7 ± 0.9 μm^2/min for DOCK2$^{-/-}$ B cells vs. 23.7 ± 4.1 μm^2/min for control cells; Fig. 2, C and D).

Table I. Motility parameters of control and DOCK2- and/or PI3Kγ-deficient T and B cells

	Control	DOCK2$^{-/-}$	Control	PI3Kγ$^{-/-}$	Control	DOCK2$^{-/-}$ × PI3Kγ$^{-/-}$
T cells						
Number of experiments	4		6		4	
Number of tracks	842	370	198	299	196	86
3D velocity (μm min^{-1})	12.6 ± 0.7	7.0 ± 0.1[a]	11.5 ± 0.8	11.0 ± 1.3	12.2 ± 1.4	6.2 ± 0.5[a]
Turning angle distribution	narrow	broad	narrow	slightly broader	narrow	broad
Motility coefficient (μm^2 min^{-1})	72.9 ± 3.7	4.8 ± 2.8[a]	70.6 ± 8.5	59.2 ± 7.3[a]	71.3 ± 4.9	3.2 ± 1.9[a]
B cells						
Number of experiments	4		6		4	
Number of tracks	133	35	134	83	243	59
3D velocity (μm min^{-1})	7.9 ± 0.8	5.2 ± 0.9[a]	8.1 ± 0.3	7.5 ± 0.7	8.3 ± 0.2	5.9 ± 0.6[a]
Turning angle distribution	narrow	broad	narrow	narrow	narrow	broad
Motility coefficient (μm^2 min^{-1})	23.7 ± 4.1	1.7 ± 0.9[a]	21.9 ± 5.2	24.3 ± 3.2	23.6 ± 5.4	2.5 ± 1.0[a]

[a]Significantly lower three-dimensional velocity or motility coefficient compared with control lymphocytes ($P < 0.05$).

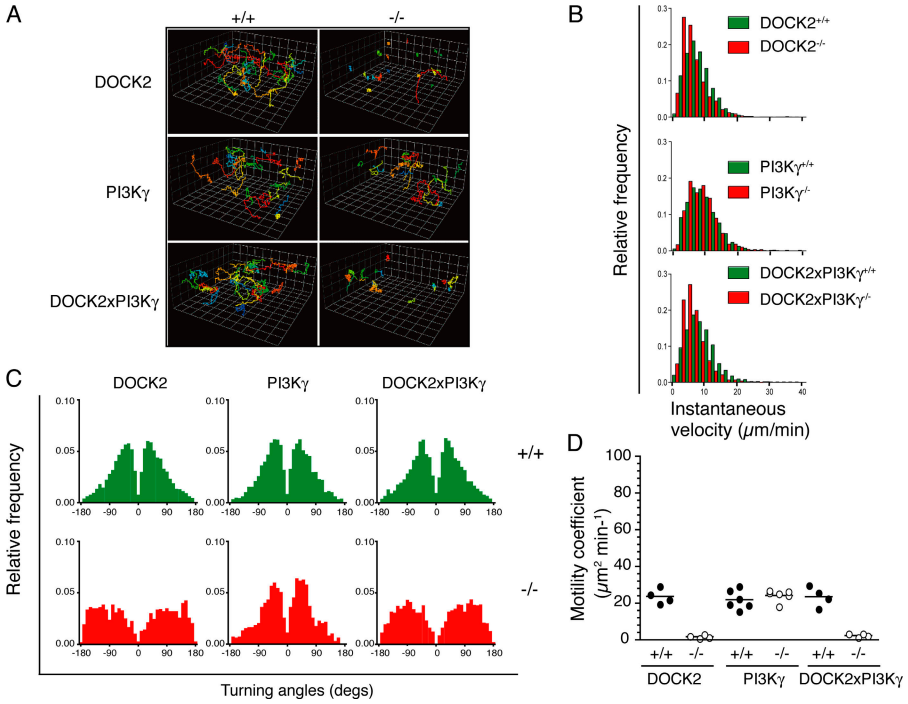

Figure 2. Follicular B cell migration in the absence of DOCK2 and PI3Kγ. Control B cells were adoptively transferred with DOCK2$^{-/-}$, PI3Kγ$^{-/-}$, or DOCK2$^{-/-}$ × PI3Kγ$^{-/-}$ B cells, and their migratory behavior was analyzed inside B cell follicles using MP-IVM as in Fig. 1. (A) Representative three-dimensional tracks of control B cells (+/+; left column), DOCK2$^{-/-}$, PI3Kγ$^{-/-}$, or DOCK2$^{-/-}$ × PI3Kγ$^{-/-}$ B cells (−/−; right column) during 30-min observation periods. Each colored line represents a single B cell track. (B) Velocity profiles of control B cells (green bars) and DOCK2$^{-/-}$, PI3Kγ$^{-/-}$, or DOCK2$^{-/-}$ × PI3Kγ$^{-/-}$ B cells (red bars). Histograms show the relative frequency distribution of different populations compared with control B cells. (C) Turning angles of control B cells (+/+; top green panel) and DOCK2$^{-/-}$, PI3Kγ$^{-/-}$, or DOCK2$^{-/-}$ × PI3Kγ$^{-/-}$ mice B cells (−/−; bottom red panel). (D) Motility coefficients of B cells in the presence or absence of DOCK2 and/or PI3Kγ. Each dot represents the motility coefficient of one experiment. Filled dots, control B cells; empty dots, genetically deficient B cells. The bars indicate mean values. The statistical analysis is summarized in Table I.

In contrast, PI3Kγ$^{-/-}$ B cell motility was indistinguishable from control B cells. A thorough analysis did not reveal significant differences in mean instantaneous three-dimensional velocity, turning angles, or motility coefficients (24.3 ± 3.2 μm^2/min for PI3Kγ$^{-/-}$ B cells vs. 21.9 ± 5.2 μm^2/min for control cells; Fig. 2, A–D). Moreover, we did not detect an additional effect when the migratory behavior of DOCK2$^{-/-}$ × PI3Kγ$^{-/-}$ B cells was compared with DOCK2$^{-/-}$ single deficient B cells (Fig. 2, A–D). In summary, these observations support a central role for DOCK2 during interstitial B cell migration (Video S6, available at http://www.jem.org/cgi/content/full/jem.20061780/DC1). The absence of PI3Kγ, on the other hand, did not affect B cell motility within lymphoid tissue.

S1P-induced protein kinase B (PKB) activation, F-actin polymerization, and migration in the absence of DOCK2 and PI3K

Efficient lymphocyte egress from PLNs depends on $S1P_1$, a $G_{\alpha i}$-coupled receptor expressed on naive lymphocytes (1, 24). The concomitant expression of CKR and $S1P_1$ on the same cell type and the involvement of DOCK2 and PI3Kγ during lymphocyte homing to PLNs and interstitial migration prompted us to investigate a role for these molecules in S1P-induced signal transduction. In cell lines, S1P has been described to induce PI3K, Rac, and ERK activation, as well as cell migration, among other downstream effects (34–36). We first evaluated PKB phosphorylation as an indirect measure for PI3K activity in control and genetically modified lymphocytes. As $S1P_1$ surface levels are highly susceptible to down-regulation by S1P in the lymph and blood (37), we allowed lymphocytes to recover $S1P_1$ expression after overnight (o.n.) incubation in fatty acid–free medium. Under these conditions, both control and genetically deficient lymphocytes exhibited comparable $S1P_1$ surface levels (Fig. S2 A, available at http://www.jem.org/cgi/content/full/jem.20061780/DC1). Upon stimulation with chemokines or S1P, phosphorylated PKB was readily detected in control lymphocytes as well as in PI3Kγ$^{-/-}$ B cells. DOCK2$^{-/-}$ lymphocytes had reduced but detectable levels of phosphorylated PKB after S1P stimulation (Fig. 3 A). In contrast, PKB did not undergo phosphorylation in PI3Kγ$^{-/-}$ T cells after chemokine or S1P addition (Fig. 3 A). These data suggest that S1P activates PKB in a PI3Kγ-dependent manner in T cells and via a different mechanism in B cells.

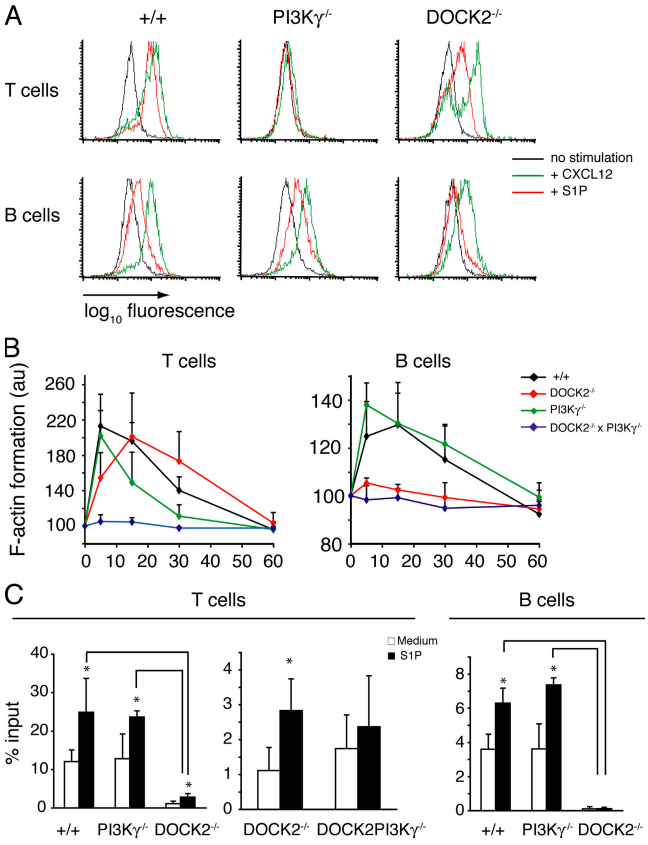

Figure 3. DOCK2 and PI3Kγ transmit signals downstream of S1P receptors. (A) Flow cytometric analysis of PKB phosphorylation 30 s after the addition of S1P (1 μM final concentration; red line) or 1 min after the addition of CXCL12 (100 nM final concentration; green line) in control, DOCK2$^{-/-}$, or PI3Kγ$^{-/-}$ T and B cells using phosphorylated PKB-specific antibody. The black line represents background staining in the absence of stimuli. (B) Flow cytometric analysis of F-actin polymerization after S1P addition (500 nM final concentration) in control, DOCK2$^{-/-}$, PI3Kγ$^{-/-}$, and DOCK2$^{-/-}$ × PI3Kγ$^{-/-}$ T and B cells. Data are presented as normalized mean fluorescence intensity of FITC-Phalloidin binding, with the "0" time point = 100. Each value corresponds to the mean ± SD of at least three independent experiments. au, arbitrary units. (C) Chemotaxis of control, DOCK2$^{-/-}$, PI3Kγ$^{-/-}$, and DOCK2$^{-/-}$ × PI3Kγ$^{-/-}$ T and B cells to 25 nM S1P for 4 h at 37°C. Significant migration to S1P over medium is marked with an asterisk ($P < 0.05$). Interconnected bars indicate significant difference ($P < 0.05$; ANOVA). Data represent mean ± SD of three independent experiments.

We next assessed Rac-mediated F-actin formation in absence of DOCK2 or PI3K. Control lymphocytes displayed a robust F-actin polymerization after S1P addition (Fig. 3 B), which was blocked by prior incubation with FTY720-P or pertussis toxin (Fig. S2 B and not depicted). Of note, the $S1P_1$-specific agonist SEW2871 also inhibited S1P-mediated F-actin formation as early as 15 min of preincubation (Fig. S2 B). We observed substantial F-actin polymerization in DOCK2$^{-/-}$ T but not B cells (Fig. 3 B). Under these conditions, F-actin formation in DOCK2$^{-/-}$ T cells was only significantly lower at the earliest time point measured (52% reduction at 5 s after S1P addition; $P < 0.05$). When F-actin polymerization was examined using freshly isolated lymphocytes, however, DOCK2-deficient T cells did not respond to S1P (Fig. S2 C), despite comparable $S1P_1$ mRNA levels as assessed by quantitative RT-PCR (not depicted).

The incomplete inhibition of F-actin formation in DOCK2-deficient T cells suggested the existence of alternative pathways. PI3K is known to mediate detectable F-actin formation in chemokine-stimulated T cells (31). When o.n. serum-starved control lymphocytes were pretreated with the PI3K inhibitor Wortmannin, S1P-induced actin polymerization at later time points (15–30 s) was significantly lower in T cells, although the initial F-actin polymerization peak was comparable to untreated cells (Fig. S2 C). S1P-triggered F-actin polymerization was also significantly reduced in PI3Kγ-deficient T cells at later time points (15–30 s; $P < 0.05$), but not at the earliest time point measured (5 s; Fig. 3 B). To assess the combined effect of DOCK2 and PI3K deficiency downstream of S1P receptors, we blocked PI3K activity in DOCK2-deficient lymphocytes. Wortmannin treatment of DOCK2$^{-/-}$ T cells abolished residual S1P-induced F-actin polymerization, suggesting that in lymphocytes, DOCK2 and PI3K independently lead to Rac activity important for actin cytoskeleton remodeling (Fig. S2 B). As predicted from this result, the combined lack of DOCK2 and PI3Kγ in T cells completely eliminated F-actin formation in vitro (Fig. 3 B).

We performed in vitro chemotaxis assays to S1P to examine the functional consequences of reduced F-actin formation in the absence of DOCK2 and PI3Kγ. Control T cells exhibited a small but reproducible migration (Fig. 3 C) that could be blocked after pretreatment with FTY720-P (not depicted), in line with previous findings (38). Despite their reduced F-actin formation, PI3Kγ$^{-/-}$ T cells migrated to S1P comparably to control T cells, whereas only rare DOCK2$^{-/-}$ T cells accumulated in the lower chamber during the chemotaxis assay (Fig. 3 C). When compared with background migration, there was nonetheless a detectable migratory response in the absence of DOCK2, which was not present in T cells lacking both DOCK2 and PI3Kγ (Fig. 3 C). In B cells, no migration was observed in the absence of DOCK2, whereas PI3Kγ deficiency did not alter migration (Fig. 3 C and Fig. S2 D). Collectively, these in vitro data implicate DOCK2 and PI3Kγ (in T cells) in the signaling cascade leading to F-actin formation and support a role for DOCK2 for efficient in vitro migration to S1P. PKB phosphorylation induced by S1P involves PI3Kγ in T cells and an alternative PI3K isoform in B cells.

Impaired lymphocyte egress from PLNs in the absence of DOCK2 but not PI3Kγ

To determine whether DOCK2 deficiency affected lymphocyte exit from PLNs in vivo, we performed egress experiments in which fluorescently labeled control and DOCK2$^{-/-}$ lymphocytes were adoptively transferred into wild-type recipient mice and allowed to accumulate in PLNs for 4 or 20 h.

To block further homing, we then administered i.v. 100 μg anti–L-selectin mAb (Mel-14), as described previously (19, 25, 33). Because DOCK2$^{-/-}$ T cells adhere well in HEV but accumulate more slowly in surrounding tissue (31, 39), mice were left for 2 h after mAb injection to allow adherent cells to either transmigrate into PLNs or to detach and reenter the circulation. As lymphocytes gradually leave PLNs via efferent lymphatic vessels, and Mel-14 treatment prevents lymph node replenishment by blood-borne lymphocytes, these assays allow for the assessment of the egress efficiency for distinct cell populations. Mice were killed 2, 12, and 24 h after mAb treatment, and the total and relative numbers of control and DOCK2$^{-/-}$ T and B cells residing inside PLNs at each time point were determined using flow cytometry to establish a retention ratio, defined as the ratio of recovered gene-deficient over control lymphocytes per each time point, corrected for input. The gradual reduction of total cell numbers recovered from PLNs after Mel-14 treatment (45% at 12 h and 85% at 24 h after mAb treatment) confirmed effective PLN homing inhibition.

As predicted, total cell numbers and the ratio of control versus DOCK2$^{-/-}$ lymphocytes recovered from PLNs indicated more efficient homing of the former population when Mel-14 was injected 4 h after cell transfer (Fig. S3 A, available at http://www.jem.org/cgi/content/full/jem.20061780/DC1). Immunohistological analysis of PLN sections revealed that under these conditions, DOCK2$^{-/-}$ cells often localized in close vicinity to HEVs, whereas control lymphocytes appeared more dispersed throughout the section (Fig. S3 C). At 12 h after mAb treatment, the absolute number of control lymphocytes inside the node experienced a gradual decrease, whereas DOCK2$^{-/-}$ T and B cell numbers remained essentially constant during this time window (Fig. S3 A). Their relative inability to leave lymphoid tissue compared with control cells was reflected by the twofold increase in the retention ratio during this period. At 24 h after mAb treatment, DOCK2$^{-/-}$ lymphocytes outnumbered control cells inside PLNs (Fig. S3 B).

As the slower egress of DOCK2-deficient lymphocytes in the above experiments may at least in part be due to their perivascular accumulation, we performed experiments in which adoptively transferred cells were allowed to accumulate in PLNs for 20 h before Mel-14 was injected to block further homing. PLN cryosection analysis confirmed that under these conditions, control and DOCK2-deficient lymphocytes colocalized in lymph node stroma (Fig. 4 D). At 2 h after mAb treatment, flow cytometry analysis of recovered adoptively transferred cells showed reduced homing of DOCK2$^{-/-}$ lymphocytes in PLNs (Fig. 4 A). When following cells for the next 24 h after transfer, DOCK2-deficient lymphocytes egressed at a slower rate from PLNs compared with control cells (Fig. 4, A and B). Although control lymphocytes had an average dwell time (determined as the time point where 50% of the initial population is found in PLNs) of ~11 h, DOCK2-deficient lymphocytes had a twofold increased dwell time of 24 h. The slower egress is reflected by

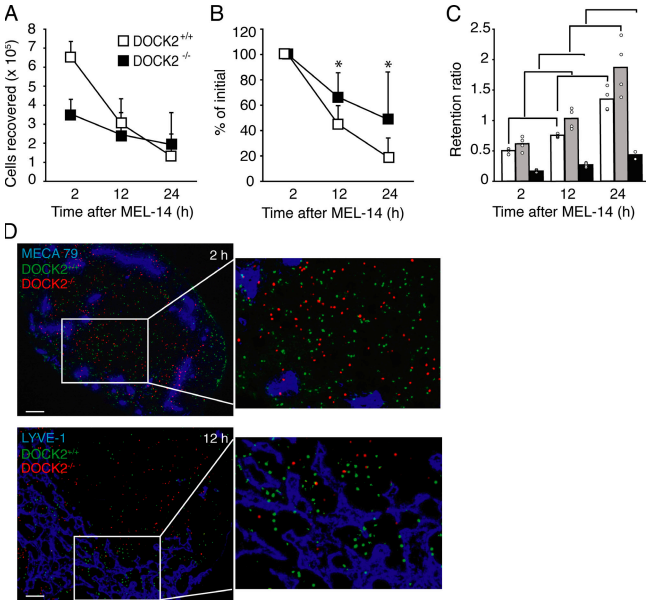

Figure 4. DOCK2 deficiency delays lymphocyte egress from PLNs. (A) Absolute numbers of control and DOCK2$^{-/-}$ lymphocytes recovered from PLNs at the indicated times after Mel-14 treatment (20 h after adoptive transfer). Fluorescently labeled control and DOCK2$^{-/-}$ lymphocytes were adoptively transferred into recipient mice, and after 20 h, further homing was blocked by the injection of Mel-14 mAb. $n = 4$ mice per time point from two independent experiments. (B) Kinetic of control and DOCK2$^{-/-}$ lymphocyte egress expressed as percent of normalized initial population. Asterisks indicate significant difference compared with control lymphocytes ($P < 0.05$). (C) Retention ratio of adoptively transferred total lymphocytes (open bars), T cells (gray bars), and B cells (filled bars) at the indicated times after Mel-14 treatment (20 h after adoptive transfer). Individual mice are represented by open circles, and bars correspond to mean values. The relative frequency of DOCK2$^{-/-}$ T and B cells increases during Mel-14 treatment, indicating slower egress kinetics. One-way ANOVA was used to determine significance between different time points. Interconnected columns are significantly different ($P < 0.05$). (D) Cryosections of PLNs isolated 2 and 12 h after Mel-14 treatment (20 h after adoptive transfer) showing distribution of CMFDA-labeled DOCK2$^{+/+}$ lymphocytes and CMTMR-labeled DOCK2$^{-/-}$ lymphocytes. HEVs are stained with anti-PNAd mAb MECA-79 in the top panel and lymphatic endothelium with LYVE-1 antibody in the bottom panel (blue). For clarity, a rectangular segment of each section has been magnified as indicated. Bar, 100 μm.

the increasing retention ratio over time in the absence of DOCK2, affecting both T and B cells (Fig. 4 C).

We performed immunohistology of PLNs to evaluate the distribution of adoptively transferred cells at 12 and 24 h after transfer. 12 h after Mel-14 treatment, 65% of control lymphocytes (of 748 total cells counted) were inside or <50 μm from lymphatic vessels, whereas only 39% of DOCK2$^{-/-}$ lymphocytes were near LYVE-1$^+$ structures (639 total cells counted; Fig. 4 D). Comparable results were obtained at 24 h after adoptive transfer, although fewer cells were present in sections (not depicted). The reduced accumulation of DOCK2-deficient cells close to lymphatic structures suggests that the absence of DOCK2 delays lymphocyte egress

without completely abolishing it. Similarly, when we isolated thoracic duct lymph and PLNs from recipient mice 36 h after adoptive transfer, approximately two to three times fewer DOCK2$^{-/-}$ T cells compared with control T cells were found in lymph when normalized to the population recovered from PLNs (not depicted).

Based on the decreased F-actin formation by PI3K$\gamma^{-/-}$ T cells in vitro, we also wanted to address whether and to what extent PI3Kγ was implicated in lymphocyte dwell time under physiological conditions. To this end, we performed similar PLN egress experiments comparing control and PI3K$\gamma^{-/-}$ lymphocytes. As reported (31, 32), we detected a small but reproducible reduction in PLN homing by PI3Kγ-deficient lymphocytes as compared with coinjected wild-type cells (Fig. 5 A). Nonetheless, the rates of control and PI3K$\gamma^{-/-}$ T and B cell egress were comparable throughout the entire observation period, as illustrated by a similar decrease in absolute cell numbers and similar retention ratios at all time points analyzed (Fig. 5, A and B). Interstitial distribution of transferred cells with respect to MECA-79$^+$ or LYVE-1$^+$ vessels was always comparable in control and PI3K$\gamma^{-/-}$ lymphocytes at all time points analyzed (not depicted).

Finally, we adoptively transferred DOCK2 × PI3Kγ-deficient lymphocytes and performed egress assays to address whether residual egress observed in DOCK2-deficient lymphocytes depended on PI3K activity. Lack of PI3Kγ did not further delay egress of DOCK2-deficient lymphocytes, identifying the absence of DOCK2 as the major cause for decreased lymphocyte egress (Fig. 5 C). Similar results were obtained when DOCK2$^{-/-}$ lymphocytes were pretreated with Wortmannin before adoptive transfer (not depicted).

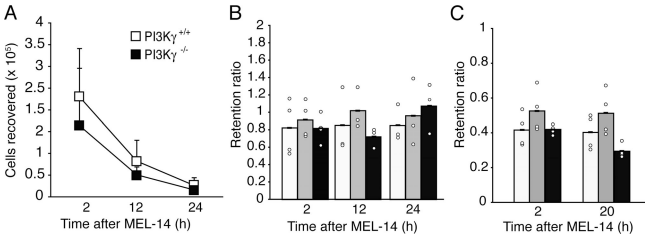

Figure 5. PI3Kγ deficiency does not affect lymphocyte egress from PLNs. (A) Total numbers of PI3K$\gamma^{+/+}$ and PI3K$\gamma^{-/-}$ cells present in PLNs at 2, 12, and 24 h after Mel-14 mAb treatment (4 h after adoptive transfer). Data represent mean ± SD from at least three mice from two independent experiments. (B) Retention ratio of PI3K$\gamma^{+/+}$ and PI3K$\gamma^{-/-}$ T and B cells at 2, 12, and 24 h after cell transfer. Each circle represents individual mice, and bars depict mean values. Shown are transferred total lymphocytes (open bars), T cells (gray bars), and B cells (filled bars) at the indicated times after Mel-14 mAb treatment. No significant difference in ratio became apparent. (C) Retention ratio of DOCK2$^{-/-}$ and DOCK2$^{-/-}$ × PI3K$\gamma^{-/-}$ T and B cells. 20 h after cell transfer, further homing was blocked by Mel-14 mAb administration, and mice were killed at 2 and 20 h later. Each circle represents individual mice, and bars depict mean values. Shown are transferred total lymphocytes (open bars), T cells (gray bars), and B cells (filled bars) at the indicated times after Mel-14 mAb treatment. Data are from two independent experiments with four mice per time point. No significant difference in ratio became apparent.

Thus, DOCK2 but not PI3Kγ deficiency increases lymph node dwell time in vivo by slowing lymphocyte egress from PLNs.

T cell motility in PLN medulla is reduced in the absence of DOCK2

Despite the reduced responsiveness of DOCK2$^{-/-}$ lymphocytes to S1P in vitro, it remained unclear whether the increased lymph node dwell time of DOCK2-deficient T cells was due to low sensitivity to S1P-mediated egress signals in addition to the overall reduced accumulation in medullary cords. We therefore directly investigated the migratory behavior of control and DOCK2-deficient T cells in the medullar region of PLNs, where S1P-dependent lymphocyte egress takes place (21, 24, 37). Explanted PLNs were immobilized with the hilus facing the objective, whereas efferent lymphatic vessels were identified by labeling with fluorescent wheat germ agglutinin (WGA), as described previously (40). We analyzed cell motility of adoptively transferred T cells 15–65 μm below the capsule in close proximity to WGA-labeled vessels during 30-min observation periods.

Control T cells exhibited continuous motility with an average speed of 8.8 ± 2.1 μm/min (Fig. 6, B and C, and Video S7, which is available at http://www.jem.org/cgi/content/full/jem.20061780/DC1). These cells occasionally entered and left the lymphatic vascular lumen (Fig. 6 A), as verified by careful assessment of volume-rendered sections (not depicted). In contrast, much fewer DOCK2-deficient T cells were observed in the medullar region, in line with our immunohistological data (Fig. 4 D). DOCK2$^{-/-}$ T cells in medullary cords were even less motile as in the paracortex (average velocity, 3.7 ± 1.6 μm/min; $P < 0.01$ compared with control T cells) and remained stationary during the observation period (Fig. 6, A–C, and Video S8, which is available at http://www.jem.org/cgi/content/full/jem.20061780/DC1). The different motility is reflected in shortened average track lengths in the absence of DOCK2 (Fig. 6 B). DOCK2 is therefore required for efficient motility near efferent lymphatic vessels in the medulla.

DISCUSSION

Observations using MP-IVM have provided important insights into the remarkable interstitial motility of lymphocytes, which migrate hundreds of micrometers every day during their long life span (10, 12–15, 28). The data presented here provide novel information about intracellular signaling factors required for efficient interstitial T and B cell motility within and egress from PLNs, and uncover a central role for the lymphocyte-expressed Rac guanine exchange factor DOCK2. First, we demonstrate that DOCK2 is needed for effective T and B cell motility inside paracortex and follicles, whereas PI3Kγ helps maintain temporal directionality during interstitial migration of T cells. Second, our findings show roles for both DOCK2 and PI3K during S1P-triggered signaling, but only DOCK2 is important for efficient egress from PLNs. In combination with previous

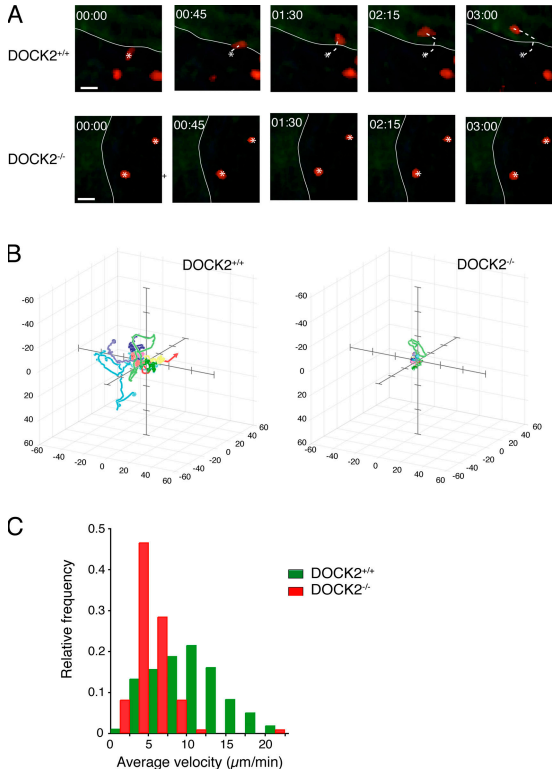

Figure 6. Medullar T cell migration in the absence of DOCK2. (A) Image sequence of control and DOCK2-deficient T cells proximal to efferent WGA$^+$ lymphatic vessels (green, outline labeled white for greater clarity). A control T cell entering WGA-labeled lymphatic vessel is shown, whereas DOCK2-deficient T cells remained stationary during the observation period. The asterisks mark the initial tracking spot. Time is in minutes and seconds. Bar, 10 μm. (B) Representative three-dimensional tracks of control and DOCK2$^{-/-}$ T cells tracked for 30 min. 10 tracks are shown for each genotype. Scale is in micrometers. (C) Velocity profile of control and DOCK2-deficient medullar T cells. 886 control T cell and 138 DOCK2$^{-/-}$ T cell tracks were analyzed from four to five independent videos.

findings regarding chemokine-induced migration (30, 31), the results presented here suggest a dominant role for DOCK2 over PI3K in intracellular signaling pathways that control central aspects of lymphocyte recirculation: homing, interstitial migration, and egress.

DOCK2 and PI3Kγ have well-described roles in CKR signaling in lymphocytes. Both contribute, in a largely independent manner, to migratory responses of T lymphocytes toward chemokine gradients in vitro (30–32, 41). The strongly reduced lymphocyte motility in the absence of DOCK2 underlines its nonredundant role for efficient cell movement induced by tissue-derived promigratory factors present in lymph stroma. Migration requires cell polarization and translocation of polarized cells (42). In vitro, DOCK2$^{-/-}$ lymphocytes show defective polarization in response to a uniform chemokine gradient (31). It is currently unclear whether within interstitial tissue DOCK2$^{-/-}$ cells fail to polarize in response to tissue-derived promigratory factors and/or whether DOCK2 is additionally required for efficient translocation. The presence of rare fast-moving DOCK2$^{-/-}$ T cells may indicate that even in the absence of DOCK2, a threshold polarization state can be achieved that allows for efficient translocation. Although the large majority of adoptively transferred cells found in PLNs correspond to phenotypically naive lymphocytes, we cannot exclude that occasional fast T cells represent subsets of central memory cells in which migration is mediated by DOCK2-independent pathways. The minor defect of PI3Kγ-deficient T cells in maintaining temporal directionality is reminiscent of the aberrant PI3Kγ$^{-/-}$ neutrophil migration toward increasing concentrations of chemoattractant. Similar to interstitially migrating T cells, PI3Kγ$^{-/-}$ neutrophils display only mildly decreased translocation speeds but are unable to form a persistent leading edge due to ineffective recruitment of pleckstrin homology domain–containing intracellular factors stabilizing the leading edge (43, 44).

The precise tissue-derived factors responsible for random lymphocyte motility within lymphoid tissue remain unknown. Numerous genetically modified mouse strains and the conspicuous expression pattern in locally distinct microenvironments point to a central role for chemokines in the overall organization of SLOs (1–3). Fibroblastic reticular cells and follicular dendritic cells form three-dimensional networks in T and B cell areas, respectively, and are the major chemokine-producing cells in lymphoid tissue (6, 45), allowing to speculate that chemokines on the surface of stromal cell networks contribute to continuous lymphocyte motility (16). In vitro, lymphocytes are generally nonmotile (12), although recent reports describe the induction of detectable random lymphocyte migration by homeostatic chemokines (17, 18). Furthermore, directed migration of activated B cells toward the T–B cell border area was found to depend on CCR7 and a CCL21 gradient (46). Similarly, the CKR CCR5 expressed on CD8 cells under proinflammatory conditions allows these cells to approach APC-CD4 clusters more efficiently (47), although factors promoting random motility were not investigated in these studies. To date, there is nonetheless no direct evidence that homeostatic chemokines such as CCL19 or CCL21 are responsible for interstitial random motility. The major factor compounding a useful in situ analysis of the role of CKR during interstitial migration lies in their central role during recruitment of blood-borne lymphocytes into SLOs. For example, genetic ablation of CCR7 or its ligands results in loss of recruitment of naive T lymphocytes into PLNs, making it difficult to analyze their role in interstitial migration (8, 9). Because chemokines present in lymph nodes induce internalization of their cognate receptors in vitro (48), an unsolved question is how these factors can promote continuous migration observed in vivo.

Besides chemokines, other tissue-derived factors may contribute to interstitial cell motility. Dendritic cells secrete the lipid mediator thromboxane A2, which enhances T cell chemokinesis in vitro by binding TP, a $G_{\alpha i}$-linked GPCR (49). Of note, TP levels are higher on T cells than on B cells, correlating with increased motility of the former population (49).

Finally, DOCK2 also acts downstream of the TCR (50), raising the possibility that non-GPCR surface receptors may participate in T cell interstitial motility. The identification of DOCK2 as a key player of continuous lymphocyte movement does therefore not further clarify the role of chemokines or additional tissue-derived factors in this process. However, recent data identified several molecules involved in GPCR signaling as important factors in promoting random B cell migration inside SLOs, as B cells lacking $G_{\alpha i2}$ or RGS1 have strongly impaired or increased interstitial motility, respectively (19). The data presented here are in line with these observations, as DOCK2 and PI3Kγ act downstream of CKR, and DOCK2$^{-/-}$ mice show evidence of markedly hypotrophic SLOs, with disturbed T and B cell compartmentalization (30). The close correlation between in vitro responsiveness to chemokines and interstitial motility in the absence of $G_{\alpha 12}$, RGS1, DOCK2, and PI3Kγ is noteworthy and suggests a strong overlap between CKR-mediated intracellular signaling pathways with those mediating random motility.

Absence of DOCK2 affects overall displacement of T and B cells, severely impairing the capacity of lymphocytes to screen extensive areas within their respective microenvironments. Recent in vitro data suggest that random motility increases efficient lymphocyte activation by facilitating encounters with CD3/28-coated beads or APCs (17, 18). An interesting question is therefore how tissue motility correlates with immune response initiation in vivo. However, studying the impact of reduced motility on immune response initiation in the absence of DOCK2 is hampered by the fact that it also acts downstream of TCR, resulting in reduced proliferation in vitro in response to irradiated splenocytes as APCs (50). It is thus difficult to directly assess the role of APC–T cell encounter efficiency for early onset or magnitude of immune responses in this model.

Lymphocyte egress from PLNs requires signals triggered by S1P, which binds to five widely expressed GPCRs, $S1P_{1–5}$ (1, 20, 34, 35). The first indication of participation of S1P receptors during lymphocyte recirculation came from studies using FTY720, an immunosuppressive agent sharing structural homology with S1P (21). Orally administered FTY720 becomes rapidly phosphorylated by S1P kinase 2 (51, 52) and, after agonistic binding to S1P receptors, induces a continuous loss of $S1P_1$ surface expression on lymphocytes through receptor internalization and degradation (23, 37). It is currently controversial whether pharmacological compounds blocking or stimulating $S1P_1$ signaling act mainly on lymphocytes or lymphatic endothelial cells, as $S1P_1$ expressed on lymphatic endothelium may participate in lymphocyte exit control through regulation of endothelial barrier properties (40, 53, 54). The interpretation of pharmacological studies is complicated by our observation that SEW2871, which acts as an $S1P_1$-specific agonist in certain cell lines (55), behaves as a functional antagonist in lymphocytes, similar to FTY720-P (Fig. S2 B). Pharmacological agonists and antagonists need thus to be carefully analyzed for their effects on primary cells to obtain a clearer picture on their effect on potential target cell populations.

Several observations clearly indicate that lymphocyte-expressed $S1P_1$ is absolutely required for physiological lymphocyte exit from lymphoid tissues. $S1P_1$-deficient mature thymocytes are retained in thymus and, upon adoptive transfer, in PLNs (24, 25, 56). In addition, a series of elegant experiments demonstrated that CD69 expressed on recently activated lymphocytes is critically involved in down-regulation of lymphocyte-expressed $S1P_1$, resulting in efficient trapping of antigen-specific lymphocytes in inflamed PLNs (57). CD69 levels do not differ between control and DOCK2-deficient lymphocytes (not depicted), excluding a role for this pathway in controlling the dwell time of DOCK2-deficient cells. As lymphocytes are able to migrate toward S1P in vitro and $S1P_1$ surface levels gradually increase with lymphocyte dwell time in PLNs (24, 37, 38), the simplest working hypothesis is that egress is a chemotactic response to S1P. This hypothesis is consistent with the recent observation that lymphocyte movement from medullar cords into lymph and blood requires S1P lyase. S1P lyase activity may create an S1P concentration gradient between lymphatic fluid and intranodal stroma, thus establishing a guidance cue for egressing lymphocytes (58). Of note, FTY720 also inhibits S1P lyase, which may further contribute to lymphocyte sequestration (59).

In line with decreased migration to S1P in vitro, multiphoton imaging showed a strongly reduced motility of medullar DOCK2-deficient T cells, which probably reflects a defect in the transmission of S1P-derived promigratory egress signals. This is supported by the observation that migration of lymphocytes in medulla is controlled by different molecular cues as paracortical migration reflected by slower migratory speed and increased susceptibility to pharmacological compounds altering S1P signaling (40, 54). It has to be cautioned, however, that our use of explanted lymph nodes results in an interruption of lymphatic flow, which may alter the physiological migratory behavior, especially concerning diapedesis into lymphatic vessels.

Our data show that in fatty acid–starved T cells stimulated by S1P, DOCK2 mediates early F-actin polymerization, whereas PI3K activity appears more important for a second, delayed wave of F-actin formation. It is interesting to note that the first wave of F-actin formation correlates with efficient migration to S1P in vitro and egress in vivo, whereas the lack of PI3K-dependent, slower F-actin formation does not strongly reduce lymphocyte migration or egress. The relation of two separate F-actin formation pathways and their physiological function is at present uncertain. T cells express mainly two of the five known S1P receptors, $S1P_1$ and $S1P_4$, although only $S1P_1$ appears to be necessary for efficient egress (1). It is possible that $S1P_1$ and $S1P_4$ show preferential intracellular coupling to DOCK2 and PI3Kγ, respectively, with DOCK2-Rac activity mediating a more robust migration. However, this needs to be experimentally addressed. It is also interesting to note that freshly isolated

DOCK2- but not PI3Kγ-deficient T cells had a strongly reduced S1P-induced F-actin formation, which may indicate that serum starvation does not represent the appropriate physiological context for measuring S1P responsiveness. Finally, it is important to note that DOCK2- and PI3K-independent pathways controlling lymphocyte exit clearly exist, which merits further investigation.

An interesting question is how lymphocytes compute various extracellular stimuli resulting in a given physiological outcome such as random interstitial motility versus egress. Our data suggest that both CKR and $S1P_1$ share important molecular players mediating migration, which could point to a central role for surface receptor expression levels, as has been suggested (37). However, in contrast to CKR and $S1P_1$ expressed in cell lines (36, 55), S1P did not induce efficient ERK phosphorylation in primary lymphocytes, indicating that $S1P_1$ and CKR share some but not all signal transduction pathways (Fig. S2 E). Within lymphoid tissue, chemokines are abundant while S1P levels are low (58, 60), and in in vitro assays, lymphocytes respond much more avidly to chemokines than to S1P. It is thus likely that in addition to regulating $S1P_1$ surface expression, other mechanisms are necessary for successful lymphocyte egress, such as a state of temporary unresponsiveness to tissue-derived factors, including chemokines. High levels of S1P, as may be present in close proximity to efferent lymphatic vessels, were found to suppress chemotactic responses of CD4 cells to homeostatic chemokines (61), providing a working model to address the balance of random interstitial motility and egress.

In summary, we show that within PLNs, T and B cells require DOCK2 for extensive screening of their respective microenvironments, while PI3Kγ helps maintaining temporal directionality during interstitial T cell migration. Furthermore, our data show an important role for DOCK2, and to a minor extent PI3K activity, for S1P-induced F-actin polymerization and migration. Reduced S1P responsiveness in the absence of DOCK2 likely contributes to the increased dwell time of DOCK2-deficient lymphocytes within PLNs. The simultaneous targeting of homing (30, 31), interstitial migration, and egress is probable to induce a permanent immunocompromised state in mice lacking DOCK2. In combination with impaired TCR signaling, it is perhaps not surprising that deletion of DOCK2 enables long-term survival in a murine model of cardiac allograft transplant (62). We therefore consider DOCK2 an interesting therapeutic target to simultaneously alter various processes controlling lymphocyte trafficking and function while not completely shutting down the immune system.

MATERIALS AND METHODS

Reagents and mice. AMCA-conjugated anti–rat IgM and Alexa350-conjugated anti–rabbit Ig were from Jackson ImmunoResearch Laboratories. Anti–LYVE-1 was purchased from RELIATech. Anti–mouse $S1P_1$ polyclonal rabbit Ig directed against the N and C terminus was provided by S. Mandala and E.J. Quackenbush (Merck Research Laboratories, Rahway, NJ). All other antibodies were from BD Biosciences or affinity purified from hybridoma supernatant (Mel-14; Nanotools). S1P and human collagen type IV were purchased from Sigma-Aldrich. CMTMR (CellTracker orange), CMFDA (CellTracker green), and CFSE were from Invitrogen. SEW2871 was from Calbiochem.

6–12-wk-old control, $DOCK2^{-/-}$, $PI3K\gamma^{-/-}$, and $DOCK2^{-/-} \times PI3K\gamma^{-/-}$ mice in a C57BL/6 background were used for all experiments. $CD45.1^+$ C57BL/6 used in some reconstitution experiments were from The Jackson Laboratory. All experiments were performed in accordance with National Institutes of Health (NIH) guidelines and approved by the Committees on Animal Care and Use of Harvard Medical School, the CBR Institute for Biomedical Research, and the Kanton of Bern.

MP-IVM of popliteal PLNs. Single cell suspensions were obtained from the PLNs, mesenteric lymph nodes, and spleens of control and genetically deficient mice. Alternatively, in some experiments (control and $PI3K\gamma^{-/-}$ T cells, and control, $DOCK2^{-/-}$, $PI3K\gamma^{-/-}$, and $DOCK2^{-/-} \times PI3K\gamma^{-/-}$ B cells), cells were isolated from irradiated $CD45.1^+$ mice reconstituted with $CD45.2^+$ bone marrow cells from control, $DOCK2^{-/-}$, $PI3K\gamma^{-/-}$, and $DOCK2^{-/-} \times PI3K\gamma^{-/-}$ mice, respectively. When required, endogenous $CD45.1^+$ cells were eliminated by negative selection with anti-CD45.1–coated magnetic beads (Miltenyi Biotec). In all experiments, T and B cell isolation was performed by negative immunomagnetic cell sorting (Miltenyi Biotec) with purity yields of >95% for T cells and >90% for B cells. Purified control, $DOCK2^{-/-}$, $PI3K\gamma^{-/-}$, or $DOCK2^{-/-} \times PI3K\gamma^{-/-}$ T or B cells were fluorescently labeled with 5 μM CFSE or 10 μM CMTMR for 15 min at 37°C, washed, and injected i.v. into sex-matched 6-wk-old C57BL/6 recipient mice. Numbers of transferred lymphocytes ($2–10 \times 10^6$ cells) were calculated according to the homing ability of each subset to allow sufficient accumulation of cells inside the node for visualization. When we checked the phenotype of control and DOCK2-deficient adoptively transferred T or B lymphocytes by flow cytometry, we found that >99% of transferred cells in PLNs were either $Thy1.2^+$ or $B220^+$, with >70% corresponding to bona fide naive lymphocytes (Fig. S1). 15–22 h after transfer, recipient mice were anesthetized and the right popliteal lymph node was surgically exposed, as described previously (33). Multiphoton imaging was performed with an Olympus BX50WI fluorescence microscope equipped with a 20× objective and a Bio-Rad Radiance 2000 MP Confocal/Multiphoton microscopy system, controlled by Lasersharp software (Bio-Rad Laboratories). For multiphoton excitation and second harmonic generation, a Ti:sapphire laser with a 10-W MilleniaXs pump laser (Tsunami; Spectra-Physics) was tuned to 800 nm. For four-dimensional analysis of cell migration, stacks of 16 square x-y sections were acquired every 15 s during 30 min with electronic zooming up to 6× to provide image volumes of 60 μm in depth. Emitted light and second harmonic signals were detected through 400/40-nm, 525/50-nm, and 620/100-nm bandpass filters with nondescanned detectors to generate three-color images. Sequences of image stacks were transformed into volume-rendered four-dimensional movies using Volocity software (Improvision), which was also used for semi-automated tracking of cell motility in three dimensions. From x, y, and z coordinates of cell centroids, parameters of cellular motility were calculated as described previously (33). In brief, the instantaneous three-dimensional velocity is the cellular velocity between two time points, whereas the turning angle describes the angle between the two velocity vectors before and after a measurement time point (12). Both parameters are determined independently for each cell track.

S1P-induced PKB and ERK phosphorylation, F-actin polymerization, and migration. Lymphocyte isolation and functional experiments were performed in RPMI supplemented with 1 mg/ml of fatty acid–free BSA, L-Gln, NaPyruvate, β-mercaptoethanol, and PenStrep (RPMI-BSA). After o.n. incubation in RPMI-BSA at 37°C, 7% CO_2, lymphocytes were stimulated with 500 nM S1P or 100 nM CXCL12, permeabilized, and incubated with anti-phosphoPKB or anti-phosphoErk (Cell Signaling Laboratories). As secondary antibodies, we used biotinylated anti–rabbit IgG (Jackson ImmunoResearch Laboratories), followed by APC-conjugated streptavidin (BD Biosciences). Comparable results were obtained using Western blot analysis (unpublished data).

Actin polymerization assays were performed as described previously (31). In brief, single cell suspensions of total lymphocytes (10^7 cells/ml) were stimulated with 500 nM S1P, and aliquots were taken at indicated time points, followed by immediate fixation in 4% paraformaldehyde for 15 min. Cells were washed with PBS and stained for Thy1.2$^+$ and B220$^+$ cells, permeabilized, labeled with FITC-Phalloidin (Invitrogen), and analyzed by flow cytometry using CELLQuest software (Becton Dickinson). In some experiments, lymphocytes were treated with 0.1 μg/ml pertussis toxin (Sigma-Aldrich), 0.5 μM Wortmannin (Calbiochem), 5 μM SEW2871, or 0.5 μM FTY720 or FTY720-P (provided by V. Brinkmann, Novartis, Basel, Switzerland, and S. Mandala and E.J. Quackenbush, respectively) for 15 min or 2 h at 37°C, 7% CO_2, before S1P stimulation.

Chemotaxis assays were performed using Transwell chambers (5-μm pore size; CoStar). Filters were coated o.n. at 4°C with a 10 μg/ml solution of human collagen type IV, washed twice with 500 μl PBS, and dried before use. Uncoated filter inserts were used with comparable results. 10^6 lymphocytes in 100 μl RPMI-BSA was placed in the top chamber and allowed to migrate to 25 nM S1P for 4 h at 37°C, 7% CO_2. This concentration was found to be optimal for both control and DOCK2$^{-/-}$ lymphocytes over a range from 10 nM to 1 μM S1P (unpublished data). The percentage of total migrated cells was determined by flow cytometry comparing with a precalibrated bead standard (Sigma-Aldrich). After migration, input and migrated populations were labeled for T and B cells to calculate percentages of subset migration.

Determination of S1P$_1$ mRNA levels and surface expression. Total RNA was isolated from freshly isolated CD4$^+$ T cells according to the manufacturer's instructions (QIAGEN). Quantitative RT-PCR was performed using the universal probe library system (Roche Applied Science). For S1P$_1$ surface labeling, lymphocytes were incubated o.n. in RPMI-BSA and labeled with anti–mouse N-terminal S1P$_1$-specific rabbit Ig, followed by biotinylated anti–rabbit Ig and streptavidin-APC. As controls, we used C-terminal S1P$_1$ or S1P$_4$-specific rabbit Ig and FTY720-P pretreatment.

Lymph node egress assays. Total lymphocytes were isolated from the spleens and PLNs of control and genetically deficient mice and fluorescently labeled using 0.3 μM CMFDA or 1.5 μM CMTMR for 45 min, 5% CO_2, 37°C in RPMI supplemented with 10% FCS, L-Gln, NaPyruvate, β-mercaptoethanol, and PenStrep (CM-R). Depending on the homing ability of different subsets, 2–4 × 10^7 cells of each cell population were mixed in 200 μl CM-R and injected i.v into age- and sex-matched C57BL/6 recipient mice. 4 or 20 h after lymphocyte transfer, mice received i.v. injections of Mel-14 (100 μg/mouse) to prevent further homing. Mice were killed 2, 12, and 24 h after mAb injection for assessment of the rate of egress of injected lymphocytes from PLNs. SLOs and blood were collected, labeled with anti-Thy1.2 and anti-B220, and the numbers of adoptively transferred T and B cells were determined using flow cytometry. For each organ, absolute numbers of each lymphocyte subset were calculated by using a precalibrated bead standard. A lymph node retention ratio was determined for each time point as the ratio of (percent recovered gene-deficient lymphocytes/percent recovered control lymphocytes) × correction factor for the input population ratio, as described previously (31). One lymph node from each mouse was snap frozen for immunohistological analysis.

Immunohistology. 8-μm sections of frozen PLNs were fixed for 10 min in 2% paraformaldehyde, washed in PBS, blocked with FCS, and stained with anti-PNAd (MECA-79) or anti–LYVE-1 antibody. AMCA-conjugated anti–rat IgM or Alexa350-conjugated anti–rabbit Ig were used as secondary antibody. Preparations were observed using a fluorescence microscope (Nikon). For determination of cell distribution, adoptively transferred lymphocytes were considered close to LYVE-1$^+$ structures at a distance of <50 μm.

Multiphoton imaging of PLN medulla. CMTMR-labeled control or DOCK2$^{-/-}$ T cells (2–10 × 10^6 cells/mouse) were adoptively transferred into C57BL/6 mice 16–24 h before isolation of PLNs (axillary, brachial, and inguinal). Explanted PLNs were labeled for 5 h with AlexaFluor488-conjugated WGA on ice as described previously (40). Labeled PLNs were carefully immobilized on a glass slide with the hilus facing up and imaged using a Trimscope MP system (LaVision) equipped with a MaiTai HP Ti:Sa laser (Spectraphysics). During image acquisition, PLNs were kept at 35–37°C and continuously superfused with oxygenated (95% O_2, 5% CO_2) bicarbonate buffered solution (130 mM NaCl, 2.5 mM KCl, 1.3 mM NaH_2PO_4, 26 mM $NaHCO_3$, 1 mM $MgCl_2$, 2 mM $CaCl_2$, and 10 mM glucose, pH 7.4, when equilibrated with a mixture of 95% O_2 and 5% CO_2). Image stacks (200 × 200 × 40 μm) between 10 and 65 μm below the lymph node surface were taken every 15 s during 30 min with a z-step size of 4 μm, using 840 nm excitation wave length. Fluorescent and second harmonic generation signals were collected using 455/50 and 525/50 bandpass filters or 560LP filters and analyzed using Volocity software. The average track velocity was calculated as total track length over tracking time.

Statistical analysis. The Student's *t* test or one-way analysis of variance (ANOVA) was used for statistical analysis (Prism or InStat; GraphPad Software). Significance was set at $P < 0.05$.

Online supplemental material. Fig. S1 shows a flow cytometric analysis of the phenotype of adoptively transferred wild-type and DOCK2$^{-/-}$ T cells. Fig. S2 shows S1P$_1$ surface expression levels of control and gene-deficient lymphocytes, as well as S1P-induced F-actin formation, B cell migration, and ERK phosphorylation. Fig. S3 depicts PLN egress of control and DOCK2$^{-/-}$ lymphocytes after an initial 4-h homing period. Supplemental videos show interstitial motility of paracortical control and DOCK2$^{-/-}$ T cells (Videos S1 and S2), control and PI3K$\gamma^{-/-}$ T cells (Video S3), control and DOCK2$^{-/-}$ × PI3K$\gamma^{-/-}$ T cells (Videos S4 and S5), and follicular control and DOCK2$^{-/-}$ B cells (Video S6). Videos S7 and S8 depict migration of medullar control and DOCK2$^{-/-}$ T cells, respectively. The online supplemental material is available at http://www.jem.org/cgi/content/full/jem.20061780/DC1.

We are grateful to Teresa de la Cueva, Luis Almonacid, and Dr. Angel Zaballos (CNB, Madrid, Spain) for excellent technical advice and help; Dr. Markus Gräler (Hannover University) and Lawrence R. Shiow (University of California, San Francisco) for useful advice on S1P experiments; Dr. Volker Brinkmann (Novartis) for providing FTY720; and Drs. Elizabeth J. Quackenbush and Suzanne Mandala (Merck) for FTY720-P, anti–mouse S1P receptor antibody, and critical reading of the manuscript.

This work was partially supported by EU grants as well as the Foundation Lilly and the Spanish Ministry of Education and Science awarded to the Department of Immunology and Oncology (CNB). This work was supported by Swiss National Foundation grant 3100-107510 and Marie Curie Excellence grant 2005-025405 (to J.V. Stein). C. Nombela-Arrieta was a recipient of EMBO short-term fellowship ASTF 181-04. T.R. Mempel received NIH training grant T32-HL-066987-04.

The authors have no conflicting financial interests.

Submitted: 18 August 2006
Accepted: 31 January 2007

REFERENCES

1. Cyster, J.G. 2005. Chemokines, sphingosine-1-phosphate, and cell migration in secondary lymphoid organs. *Annu. Rev. Immunol.* 23:127–159.
2. von Andrian, U.H., and T.R. Mempel. 2003. Homing and cellular traffic in lymph nodes. *Nat. Rev. Immunol.* 3:867–878.
3. Stein, J.V., and C. Nombela-Arrieta. 2005. Chemokine control of lymphocyte trafficking: a general overview. *Immunology.* 116:1–12.
4. Scimone, M.L., T.W. Felbinger, I.B. Mazo, J.V. Stein, U.H. Von Andrian, and W. Weninger. 2004. CXCL12 mediates CCR7-independent homing of central memory cells, but not naive T cells, in peripheral lymph nodes. *J. Exp. Med.* 199:1113–1120.
5. Ebisuno, Y., T. Tanaka, N. Kanemitsu, H. Kanda, K. Yamaguchi, T. Kaisho, S. Akira, and M. Miyasaka. 2003. Cutting edge: the B cell chemokine CXC chemokine ligand 13/B lymphocyte chemoattractant is expressed in the high endothelial venules of lymph nodes and Peyer's

patches and affects B cell trafficking across high endothelial venules. *J. Immunol.* 171:1642–1646.
6. Ansel, K.M., V.N. Ngo, P.L. Hyman, S.A. Luther, R. Forster, J.D. Sedgwick, J.L. Browning, M. Lipp, and J.G. Cyster. 2000. A chemokine-driven positive feedback loop organizes lymphoid follicles. *Nature*. 406:309–314.
7. Förster, R., A.E. Mattis, E. Kremmer, E. Wolf, G. Brem, and M. Lipp. 1996. A putative chemokine receptor, BLR1, directs B cell migration to defined lymphoid organs and specific anatomic compartments of the spleen. *Cell*. 87:1037–1047.
8. Förster, R., A. Schubel, D. Breitfeld, E. Kremmer, I. Renner-Muller, E. Wolf, and M. Lipp. 1999. CCR7 coordinates the primary immune response by establishing functional microenvironments in secondary lymphoid organs. *Cell*. 99:23–33.
9. Nakano, H., T. Tamura, T. Yoshimoto, H. Yagita, M. Miyasaka, E.C. Butcher, H. Nariuchi, T. Kakiuchi, and A. Matsuzawa. 1997. Genetic defect in T lymphocyte-specific homing into peripheral lymph nodes. *Eur. J. Immunol.* 27:215–221.
10. Bousso, P., and E.A. Robey. 2004. Dynamic behavior of T cells and thymocytes in lymphoid organs as revealed by two-photon microscopy. *Immunity*. 21:349–355.
11. Miller, M.J., S.H. Wei, I. Parker, and M.D. Cahalan. 2002. Two-photon imaging of lymphocyte motility and antigen response in intact lymph node. *Science*. 296:1869–1873.
12. Sumen, C., T.R. Mempel, I.B. Mazo, and U.H. von Andrian. 2004. Intravital microscopy: visualizing immunity in context. *Immunity*. 21:315–329.
13. Wei, S.H., I. Parker, M.J. Miller, and M.D. Cahalan. 2003. A stochastic view of lymphocyte motility and trafficking within the lymph node. *Immunol. Rev.* 195:136–159.
14. Dustin, M.L. 2004. Stop and go traffic to tune T cell responses. *Immunity*. 21:305–314.
15. Huang, A.Y., H. Qi, and R.N. Germain. 2004. Illuminating the landscape of in vivo immunity: insights from dynamic in situ imaging of secondary lymphoid tissues. *Immunity*. 21:331–339.
16. Bajénoff, M., J.G. Egen, L.Y. Koo, J.P. Laugier, F. Brau, N. Glaichenhaus, and R.N. Germain. 2006. Stromal cell networks regulate lymphocyte entry, migration, and territoriality in lymph nodes. *Immunity*. 25:989–1001.
17. Kaiser, A., E. Donnadieu, J.P. Abastado, A. Trautmann, and A. Nardin. 2005. CC chemokine ligand 19 secreted by mature dendritic cells increases naive T cell scanning behavior and their response to rare cognate antigen. *J. Immunol.* 175:2349–2356.
18. Stachowiak, A.N., Y. Wang, Y.C. Huang, and D.J. Irvine. 2006. Homeostatic lymphoid chemokines synergize with adhesion ligands to trigger T and B lymphocyte chemokinesis. *J. Immunol.* 177:2340–2348.
19. Han, S.B., C. Moratz, N.N. Huang, B. Kelsall, H. Cho, C.S. Shi, O. Schwartz, and J.H. Kehrl. 2005. Rgs1 and Gnai2 regulate the entrance of B lymphocytes into lymph nodes and B cell motility within lymph node follicles. *Immunity*. 22:343–354.
20. Rosen, H., G. Sanna, and C. Alfonso. 2003. Egress: a receptor-regulated step in lymphocyte trafficking. *Immunol. Rev.* 195:160–177.
21. Mandala, S., R. Hajdu, J. Bergstrom, E. Quackenbush, J. Xie, J. Milligan, R. Thornton, G.J. Shei, D. Card, C. Keohane, et al. 2002. Alteration of lymphocyte trafficking by sphingosine-1-phosphate receptor agonists. *Science*. 296:346–349.
22. Brinkmann, V., M.D. Davis, C.E. Heise, R. Albert, S. Cottens, R. Hof, C. Bruns, E. Prieschl, T. Baumruker, P. Hiestand, et al. 2002. The immune modulator FTY720 targets sphingosine 1-phosphate receptors. *J. Biol. Chem.* 277:21453–21457.
23. Gräler, M.H., and E.J. Goetzl. 2004. The immunosuppressant FTY720 down-regulates sphingosine 1-phosphate G-protein-coupled receptors. *FASEB J.* 18:551–553.
24. Matloubian, M., C.G. Lo, G. Cinamon, M.J. Lesneski, Y. Xu, V. Brinkmann, M.L. Allende, R.L. Proia, and J.G. Cyster. 2004. Lymphocyte egress from thymus and peripheral lymphoid organs is dependent on S1P receptor 1. *Nature*. 427:355–360.
25. Halin, C., M.L. Scimone, R. Bonasio, J.M. Gauguet, T.R. Mempel, E. Quackenbush, R.L. Proia, S. Mandala, and U.H. von Andrian. 2005. The S1P-analog FTY720 differentially modulates T cell homing via HEV: T cell-expressed S1P1 amplifies integrin activation in peripheral lymph nodes but not in Peyer's patches. *Blood*. 106:1314–1322.
26. Brugnera, E., L. Haney, C. Grimsley, M. Lu, S.F. Walk, A.C. Tosello-Trampont, I.G. Macara, H. Madhani, G.R. Fink, and K.S. Ravichandran. 2002. Unconventional Rac-GEF activity is mediated through the Dock180-ELMO complex. *Nat. Cell Biol.* 4:574–582.
27. Cote, J.F., and K. Vuori. 2002. Identification of an evolutionarily conserved superfamily of DOCK180-related proteins with guanine nucleotide exchange activity. *J. Cell Sci.* 115:4901–4913.
28. Reif, K., and J. Cyster. 2002. The CDM protein DOCK2 in lymphocyte migration. *Trends Cell Biol.* 12:368–373.
29. Etienne-Manneville, S., and A. Hall. 2002. Rho GTPases in cell biology. *Nature*. 420:629–635.
30. Fukui, Y., O. Hashimoto, T. Sanui, T. Oono, H. Koga, M. Abe, A. Inayoshi, M. Noda, M. Oike, T. Shirai, and T. Sasazuki. 2001. Haematopoietic cell-specific CDM family protein DOCK2 is essential for lymphocyte migration. *Nature*. 412:826–831.
31. Nombela-Arrieta, C., R.A. Lacalle, M.C. Montoya, Y. Kunisaki, D. Megias, M. Marques, A.C. Carrera, S. Manes, Y. Fukui, A.C. Martinez, and J.V. Stein. 2004. Differential requirements for DOCK2 and phosphoinositide-3-kinase gamma during T and B lymphocyte homing. *Immunity*. 21:429–441.
32. Reif, K., K. Okkenhaug, T. Sasaki, J.M. Penninger, B. Vanhaesebroeck, and J.G. Cyster. 2004. Cutting edge: differential roles for phosphoinositide 3-kinases, p110gamma and p110delta, in lymphocyte chemotaxis and homing. *J. Immunol.* 173:2236–2240.
33. Mempel, T.R., S.E. Henrickson, and U.H. Von Andrian. 2004. T-cell priming by dendritic cells in lymph nodes occurs in three distinct phases. *Nature*. 427:154–159.
34. Spiegel, S., and S. Milstien. 2002. Sphingosine 1-phosphate, a key cell signaling molecule. *J. Biol. Chem.* 277:25851–25854.
35. Spiegel, S., and S. Milstien. 2003. Sphingosine-1-phosphate: an enigmatic signalling lipid. *Nat. Rev. Mol. Cell Biol.* 4:397–407.
36. Durand, C.A., J. Westendorf, K.W. Tse, and M.R. Gold. 2006. The Rap GTPases mediate CXCL13- and sphingosine1-phosphate-induced chemotaxis, adhesion, and Pyk2 tyrosine phosphorylation in B lymphocytes. *Eur. J. Immunol.* 36:2235–2249.
37. Lo, C.G., Y. Xu, R.L. Proia, and J.G. Cyster. 2005. Cyclical modulation of sphingosine-1-phosphate receptor 1 surface expression during lymphocyte recirculation and relationship to lymphoid organ transit. *J. Exp. Med.* 201:291–301.
38. Graeler, M., and E.J. Goetzl. 2002. Activation-regulated expression and chemotactic function of sphingosine 1-phosphate receptors in mouse splenic T cells. *FASEB J.* 16:1874–1878.
39. Shulman, Z., R. Pasvolsky, E. Woolf, V. Grabovsky, S.W. Feigelson, N. Erez, Y. Fukui, and R. Alon. 2006. DOCK2 regulates chemokine-triggered lateral lymphocyte motility but not transendothelial migration. *Blood*. 108:2150–2158.
40. Wei, S.H., H. Rosen, M.P. Matheu, M.G. Sanna, S.K. Wang, E. Jo, C.H. Wong, I. Parker, and M.D. Cahalan. 2005. Sphingosine 1-phosphate type 1 receptor agonism inhibits transendothelial migration of medullary T cells to lymphatic sinuses. *Nat. Immunol.* 6: 1228–1235.
41. Ward, S.G. 2004. Do phosphoinositide 3-kinases direct lymphocyte navigation? *Trends Immunol.* 25:67–74.
42. Mañes, S., R. Ana Lacalle, C. Gomez-Mouton, and A.C. Martínez. 2003. From rafts to crafts: membrane asymmetry in moving cells. *Trends Immunol.* 24:320–326.
43. Hannigan, M., L. Zhan, Z. Li, Y. Ai, D. Wu, and C.K. Huang. 2002. Neutrophils lacking phosphoinositide 3-kinase gamma show loss of directionality during N-formyl-Met-Leu-Phe-induced chemotaxis. *Proc. Natl. Acad. Sci. USA*. 99:3603–3608.
44. Li, Z., M. Hannigan, Z. Mo, B. Liu, W. Lu, Y. Wu, A.V. Smrcka, G. Wu, L. Li, M. Liu, et al. 2003. Directional sensing requires G beta gamma-mediated PAK1 and PIX alpha-dependent activation of Cdc42. *Cell*. 114:215–227.
45. Luther, S.A., H.L. Tang, P.L. Hyman, A.G. Farr, and J.G. Cyster. 2000. Coexpression of the chemokines ELC and SLC by T zone stromal cells

and deletion of the ELC gene in the plt/plt mouse. *Proc. Natl. Acad. Sci. USA*. 97:12694–12699.
46. Okada, T., M.J. Miller, I. Parker, M.F. Krummel, M. Neighbors, S.B. Hartley, A. O'Garra, M.D. Cahalan, and J.G. Cyster. 2005. Antigen-engaged B cells undergo chemotaxis toward the T zone and form motile conjugates with helper T cells. *PLoS Biol.* 3:e150.
47. Castellino, F., A.Y. Huang, G. Altan-Bonnet, S. Stoll, C. Scheinecker, and R.N. Germain. 2006. Chemokines enhance immunity by guiding naive CD8+ T cells to sites of CD4+ T cell-dendritic cell interaction. *Nature*. 440:890–895.
48. Bardi, G., M. Lipp, M. Baggiolini, and P. Loetscher. 2001. The T cell chemokine receptor CCR7 is internalized on stimulation with ELC, but not with SLC. *Eur. J. Immunol.* 31:3291–3297.
49. Kabashima, K., T. Murata, H. Tanaka, T. Matsuoka, D. Sakata, N. Yoshida, K. Katagiri, T. Kinashi, T. Tanaka, M. Miyasaka, et al. 2003. Thromboxane A2 modulates interaction of dendritic cells and T cells and regulates acquired immunity. *Nat. Immunol.* 4:694–701.
50. Sanui, T., A. Inayoshi, M. Noda, E. Iwata, M. Oike, T. Sasazuki, and Y. Fukui. 2003. DOCK2 is essential for antigen-induced translocation of TCR and lipid rafts, but not PKC-theta and LFA-1, in T cells. *Immunity*. 19:119–129.
51. Kharel, Y., S. Lee, A.H. Snyder, L. Sheasley-O'neill, M.A. Morris, Y. Setiady, R. Zhu, M.A. Zigler, T.L. Burcin, K. Ley, et al. 2005. Sphingosine kinase 2 is required for modulation of lymphocyte traffic by FTY720. *J. Biol. Chem.* 280:36865–36872.
52. Zemann, B., B. Kinzel, M. Muller, R. Reuschel, D. Mechtcheriakova, N. Urtz, F. Bornancin, T. Baumruker, and A. Billich. 2006. Sphingosine kinase type 2 is essential for lymphopenia induced by the immunomodulatory drug FTY720. *Blood*. 107:1454–1458.
53. Singer, I.I., M. Tian, L.A. Wickham, J. Lin, S.S. Matheravidathu, M.J. Forrest, S. Mandala, and E.J. Quackenbush. 2005. Sphingosine-1-phosphate agonists increase macrophage homing, lymphocyte contacts, and endothelial junctional complex formation in murine lymph nodes. *J. Immunol.* 175:7151–7161.
54. Sanna, M.G., S.K. Wang, P.J. Gonzalez-Cabrera, A. Don, D. Marsolais, M.P. Matheu, S.H. Wei, I. Parker, E. Jo, W.C. Cheng, et al. 2006. Enhancement of capillary leakage and restoration of lymphocyte egress by a chiral S1P(1) antagonist in vivo. *Nat. Chem. Biol.* 2:434–441.
55. Jo, E., M.G. Sanna, P.J. Gonzalez-Cabrera, S. Thangada, G. Tigyi, D.A. Osborne, T. Hla, A.L. Parrill, and H. Rosen. 2005. $S1P_1$-selective in vivo-active agonists from high-throughput screening: off-the-shelf chemical probes of receptor interactions, signaling, and fate. *Chem. Biol.* 12:703–715.
56. Allende, M.L., J.L. Dreier, S. Mandala, and R.L. Proia. 2004. Expression of the sphingosine 1-phosphate receptor, $S1P_1$, on T-cells controls thymic emigration. *J. Biol. Chem.* 279:15396–15401.
57. Shiow, L.R., D.B. Rosen, N. Brdickova, Y. Xu, J. An, L.L. Lanier, J.G. Cyster, and M. Matloubian. 2006. CD69 acts downstream of interferon-alpha/beta to inhibit $S1P_1$ and lymphocyte egress from lymphoid organs. *Nature*. 440:540–544.
58. Schwab, S.R., J.P. Pereira, M. Matloubian, Y. Xu, Y. Huang, and J.G. Cyster. 2005. Lymphocyte sequestration through S1P lyase inhibition and disruption of S1P gradients. *Science*. 309:1735–1739.
59. Bandhuvula, P., Y.Y. Tam, B. Oskouian, and J.D. Saba. 2005. The immune modulator FTY720 inhibits sphingosine-1-phosphate lyase activity. *J. Biol. Chem.* 280:33697–33700.
60. Stein, J.V., A. Rot, Y. Luo, M. Narasimhaswamy, H. Nakano, M.D. Gunn, A. Matsuzawa, E.J. Quackenbush, M.E. Dorf, and U.H. von Andrian. 2000. The CC chemokine thymus-derived chemotactic agent 4 (TCA-4, secondary lymphoid tissue chemokine, 6Ckine, exodus-2) triggers lymphocyte function–associated antigen 1–mediated arrest of rolling T lymphocytes in peripheral lymph node high endothelial venules. *J. Exp. Med.* 191:61–76.
61. Graeler, M., G. Shankar, and E.J. Goetzl. 2002. Cutting edge: suppression of T cell chemotaxis by sphingosine 1-phosphate. *J. Immunol.* 169:4084–4087.
62. Jiang, H., F. Pan, L.M. Erickson, M.S. Jang, T. Sanui, Y. Kunisaki, T. Sasazuki, M. Kobayashi, and Y. Fukui. 2005. Deletion of DOCK2, a regulator of the actin cytoskeleton in lymphocytes, suppresses cardiac allograft rejection. *J. Exp. Med.* 202:1121–1130.